



**HAL**  
open science

## Core Flow Modelling Assumptions

Ciarán Beggan, Kathy Whaler

► **To cite this version:**

Ciarán Beggan, Kathy Whaler. Core Flow Modelling Assumptions. *Physics of the Earth and Planetary Interiors*, 2008, 167 (3-4), pp.217. <10.1016/j.pepi.2008.04.011>. <hal-00532145>

**HAL Id: hal-00532145**

**<https://hal.science/hal-00532145v1>**

Submitted on 4 Nov 2010

**HAL** is a multi-disciplinary open access archive for the deposit and dissemination of scientific research documents, whether they are published or not. The documents may come from teaching and research institutions in France or abroad, or from public or private research centers.

L'archive ouverte pluridisciplinaire **HAL**, est destinée au dépôt et à la diffusion de documents scientifiques de niveau recherche, publiés ou non, émanant des établissements d'enseignement et de recherche français ou étrangers, des laboratoires publics ou privés.



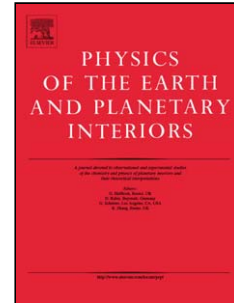
HAL Authorization

## Accepted Manuscript

Title: Core Flow Modelling Assumptions

Authors: Ciarán Beggan, Kathy Whaler

PII: S0031-9201(08)00081-2  
DOI: doi:10.1016/j.pepi.2008.04.011  
Reference: PEPI 4932



To appear in: *Physics of the Earth and Planetary Interiors*

Received date: 15-10-2007  
Revised date: 21-4-2008  
Accepted date: 23-4-2008

Please cite this article as: Beggan, C., Whaler, K., Core Flow Modelling Assumptions, *Physics of the Earth and Planetary Interiors* (2007), doi:10.1016/j.pepi.2008.04.011

This is a PDF file of an unedited manuscript that has been accepted for publication. As a service to our customers we are providing this early version of the manuscript. The manuscript will undergo copyediting, typesetting, and review of the resulting proof before it is published in its final form. Please note that during the production process errors may be discovered which could affect the content, and all legal disclaimers that apply to the journal pertain.

# Core Flow Modelling Assumptions

Ciarán Beggan<sup>\*</sup>, Kathy Whaler

*School of GeoSciences, University of Edinburgh, Edinburgh EH9 3JW, UK*

---

## Abstract

Modelling of core flows at the core-mantle boundary from secular variation requires a range of both physical and mathematical assumptions in order to derive a solution. We investigate the role of certain assumptions and an  $L_1$  norm iterative inversion method to derive core flow models. Using three datasets of secular variation, we separate the effects of: (a) the assignment of observation errors through the data covariance matrix, (b) the *a priori* constraints placed upon the solution and (c) the type of flow regime assumed to be present in the core. Flow is calculated directly from the time derivatives of the  $X$ ,  $Y$  and  $Z$  components of ground-based observatories rather than Gauss coefficients of the secular variation. We find the  $L_1$  iterative method improves the fit of the secular variation generated by the flow models to the observed data, compared to the  $L_2$  norm (least-squares) method. Using this method, we find a new class of flow solutions explaining the secular variation: purely poloidal flows, which fit the input data adequately, and, for one of our datasets, better than toroidal-only flows. The patterns of motions is very different from that seen in previous flow models, which are dominated by their toroidal component.

*Key words:* Core Flow, Geomagnetic Field, Regularisation, Secular Variation

---

## 1 **1 Introduction**

2 The Earth's main magnetic field is generally accepted to be generated and  
3 sustained by dynamo action associated with the motion of the electrically  
4 conducting fluid outer core. The main field evolves slowly over time; the grad-  
5 ual decadal timescale change of the main field is known as the secular variation  
6 (SV). Whether and how the evolution of the field over these timescales can be  
7 used to constrain the nature of the fluid motion has been a matter of on-going  
8 research for several decades. Work by Roberts and Scott (1965) formulated  
9 the problem of determining flow along the core-mantle boundary from mea-  
10 surements of SV, which was implemented by e.g. Kahle et al. (1967).

11 Under the main assumption, termed the frozen-flux approximation, that the  
12 SV of the main field is due to the simple advection of the field lines through  
13 fluid motion, disregarding any effects of diffusion (Roberts and Scott, 1965).  
14 The neglect of diffusion is justified by examining the behaviour of the field  
15 at large horizontal scales over short time intervals. However, there are short-  
16 comings to this assumption which are discussed in, for example, Gubbins and  
17 Kelly (1996), Braginsky and LeMouél (1993) and Love (1999). Furthermore,  
18 even under the frozen-flux assumption, deducing the flow velocity from the  
19 field and SV cannot be achieved uniquely, as there are entire classes of flow  
20 which do not generate any detectable SV outside the core (Backus, 1968).  
21 Therefore, further assumptions are made about the type of flow at the core-  
22 mantle boundary (CMB), to reduce the inherent non-uniqueness. Examples  
23 of non-uniqueness reducing assumptions include steady flows (Voorhies and

---

\* Corresponding author.

*Email address:* [ciaran.beggan@ed.ac.uk](mailto:ciaran.beggan@ed.ac.uk) (Ciarán Beggan).

24 Backus, 1985), toroidal-only (Whaler, 1980), tangentially geostrophic (Hills,  
25 1979; Le Mouél, 1984) or flows with a particular helicity (Amit and Olson,  
26 2004). Further assumptions must be made to produce a tractable problem,  
27 since only a finite quantity of inaccurate data is available. In particular, the  
28 flow is truncated at a large scale and a regularised solution is calculated via a  
29 damping (smoothing) parameter.

30 We wish to examine the role that underlying assumptions can have on the  
31 resulting core flow models. The past decade has seen a vast improvement in  
32 the global quality and quantity of data from satellite measurements. However,  
33 in this study we employ data from ground-based observatories, in order to  
34 calculate directly observed SV. This allows us to disregard any concern about  
35 how to account for the temporal discontinuity in satellite data for any partic-  
36 ular point on the Earth's surface. Contamination from sources external to the  
37 observatory at ground level are well understood. At satellite altitudes, these  
38 sources can be internal (as well as external) to the orbit, complicating their  
39 removal. In contrast to most other studies, we invert SV calculated from obser-  
40 vatory data – rather than spherical harmonic model coefficients – to compute  
41 flow model coefficients. This allows a more rigorous test of flow assumptions  
42 made, and incorporation of realistic data uncertainties.

43 This paper examines the results of comparisons between combined and toroidal-  
44 only flows to model the observed SV, using a one-norm minimisation inversion  
45 technique, initially imposing a minimum global root-mean-square (RMS) flow  
46 velocity constraint. Poloidal-only flows were also examined, for completeness,  
47 throwing up a number of interesting results which we will elucidate upon be-  
48 low. Further, we highlight the competing effects of the various assumptions to  
49 control the final flow model.

## 50 2 Method

51 The inverse problem of deriving a CMB flow model from observed SV data is  
 52 typically approached through relating spherical harmonic representations of  
 53 the Main Field, SV, and flow (e.g. Kahle et al., 1967; Whaler, 2007). As the  
 54 horizontal velocity averages to zero over the CMB with the radial component  
 55 across the boundary vanishing, the flow can be expressed in terms of poloidal  
 56 ( $s$ ) and toroidal ( $t$ ) scalars that can be expanded in spherical harmonics. Their  
 57 coefficients, stored in a vector  $\mathbf{m}$ , are the flow model coefficients whose values  
 58 we seek using a regularised inversion approach.

59 Spherical harmonic SV coefficients ordered in a vector ( $\dot{\mathbf{g}}$ ) are related to flow  
 60 coefficients by  $\dot{\mathbf{g}} = \mathbf{B}\mathbf{m}$  where the elements of  $\mathbf{B}$  are linear combinations  
 61 of Elsasser and Gaunt integrals, whose multipliers depend on the main field  
 62 coefficients. The vector  $\dot{\mathbf{g}}$  is related to the SV data on the surface of the Earth  
 63 by  $\mathbf{d} = \mathbf{Y}\dot{\mathbf{g}}$ . Here, the elements of the data vector,  $\mathbf{d}$ , are the observed SV  
 64 components (e.g.  $\dot{X}$ ,  $\dot{Y}$  and  $\dot{Z}$ , where  $X$ ,  $Y$  and  $Z$  denote the North, East and  
 65 vertically downwards respectively) expressed in spherical polar coordinates.  
 66  $\mathbf{Y}$  has elements which are multiples of spherical harmonics and their  $\theta$  and  
 67  $\phi$  derivatives. Thus, including the observational error ( $\mathbf{e}$ ), the linear inverse  
 68 problem becomes:

$$69 \quad \mathbf{d} = \mathbf{Y}\dot{\mathbf{g}} + \mathbf{e} = \mathbf{YB}\mathbf{m} + \mathbf{e} = \mathbf{A}\mathbf{m} + \mathbf{e} \quad (1)$$

70 We determine a model by regularised inversion, minimising an objective func-  
 71 tion combining the size, or norm, of the error vector (the error norm), and a  
 72 measure of ‘complexity’ or ‘smoothness’ of the solution (the solution norm).  
 73 We use both the  $L_1$  (or Laplacian) norm, which minimises the absolute sum of

74 the errors, and the standard  $L_2$  least-squares formulation. Errors in the mea-  
 75 surements can often be correlated, so a data covariance matrix (denoted  $\mathbf{C}_e$ ),  
 76 where the diagonal elements are the variances of the data, is used to capture  
 77 this information.

78  $L_2$  minimisation gives

$$79 \quad \hat{\mathbf{m}} = (\mathbf{A}^T \mathbf{C}_e^{-1} \mathbf{A} + \lambda \mathbf{D})^{-1} \mathbf{A}^T \mathbf{C}_e^{-1} \mathbf{d} \quad (2)$$

80 where  $\mathbf{D}$  is the regularisation matrix which is used to impose ‘smoothness’. A  
 81 damping parameter,  $\lambda$ , acts to control the importance attached to fitting the  
 82 data versus the imposition of a smooth solution. Regularisation also ensures  
 83 numerical stability of the inversion and convergence when the spherical har-  
 84 monic series for  $\mathbf{m}$  is truncated. In this study, the flow vector  $\mathbf{m}$ , the main  
 85 field model  $\mathbf{g}$  and the intermediate SV model  $\dot{\mathbf{g}}$  are truncated at degree  $l = 14$ .

86 Walker and Jackson (2000) provide the motivation to calculate the model by  
 87 an iterative one-norm minimisation method instead. In particular, they offer  
 88 empirical evidence that the distribution of residuals from a historical magnetic  
 89 dataset comprising vector, scalar and directional data is well-described by  
 90 a double-Laplacian probability distribution. Note that Walker and Jackson  
 91 (2000) modelled the magnetic field itself, rather than CMB flow, with data  
 92 being main field rather than SV observations. Here, we examine whether the  
 93 same is true of the distribution of SV residuals.

94 We use Walker and Jackson’s (2000) implementation of the one-norm solution.  
 95 The residual errors from the previous iteration are used to specify an additional  
 96 diagonal matrix  $\mathbf{R}$ , whose elements are  $R_{ii} = \sqrt{2}/|e_i|$ , where  $e_i$  is the residual  
 97 of the  $i$ th datum.  $\mathbf{R}$  is recalculated at each iteration, hence the data are

iteratively re-weighted, reducing the influence of outliers. Relabelling  $\mathbf{C}_e^{-1}$  as  $\mathbf{E}$  (to maintain consistency with the notation used in Walker and Jackson (2000)), the iterative regularised one-norm solution can be written as:

$$\hat{\mathbf{m}}_{i+1} = (\mathbf{A}^T \mathbf{E}^T \mathbf{R} \mathbf{E} \mathbf{A} + \lambda \mathbf{D})^{-1} (\mathbf{A}^T \mathbf{E}^T \mathbf{R} \mathbf{E} \mathbf{d}) \quad (3)$$

In this study, two formulations of  $\mathbf{D}$  are used, both of which measure quadratic norms of the flow. The ‘strong velocity norm’ of Bloxham (1988) is a global measure of the flow complexity, whose square is

$$\begin{aligned} \mathbf{m}^T \mathbf{Q} \mathbf{m} &= \oint_{CMB} \left[ (\nabla_h^2 u_\theta)^2 + (\nabla_h^2 u_\phi)^2 \right] dS \\ &= 4\pi \sum_l \frac{[l(l+1)]^3}{2l+1} \sum_{m=0}^l [(t_l^m)^2 + (s_l^m)^2] \end{aligned} \quad (4)$$

where  $u_\theta$  and  $u_\phi$  are the horizontal flow components.

An alternative is to minimise the CMB RMS SV. This is typically applied when undertaking regularised inversion for SV coefficients (Gubbins, 1983), but can also be used for flow modelling (Whaler, 1986). It imposes smoothness on the SV predicted by the flow rather than the flow itself. Let  $a$  be the Earth’s radius,  $c$  the radius of the CMB, and with  $\{\dot{g}_l^m, \dot{h}_l^m\}$  the Gauss coefficients of the SV, the square of this solution norm can be defined as:

$$\begin{aligned} \dot{\mathbf{g}}^T \dot{\mathbf{Q}} \dot{\mathbf{g}} &= \mathbf{m}^T \mathbf{B}^T \mathbf{B} \mathbf{m} \\ &= \oint_{CMB} \dot{B}_r^2 d\Omega = 4\pi \sum_l \left(\frac{a}{c}\right)^{2l+4} \frac{(l+2)^2}{2l+1} \\ &\quad \times \sum_{m=0}^l (\dot{g}_l^m + \dot{h}_l^m)^2 \end{aligned} \quad (5)$$

112

Equations (4) and (5) can be combined or used separately as required –  $\mathbf{Q}$  or

114  $\mathbf{B}^T \mathbf{B}$  replace  $\mathbf{D}$  in (3), e.g.  $\mathbf{D}$  is diagonal with elements  $l(l+3)^3/(2l+1)$  for  
 115 (4).

116 The ‘fit’ of the flow models to the observed data can be measured via the one-  
 117 norm ( $L_1$ ) and two-norm ( $L_2$ ) measures of the error residuals defined (where  
 118  $i$  is the number of observations) as:

$$119 \quad L_1 = \sum_{i=1}^N |e_i| \quad \text{and} \quad L_2 = \sqrt{\sum_{i=1}^N (e_i)^2} \quad (6)$$

120 It is important also to test whether the residuals conform better to a Gaussian  
 121 or double-Laplacian distribution.

### 122 **3 Observatory Data**

123 Three separate SV datasets were considered, all consisting of  $\dot{X}$ ,  $\dot{Y}$  and  $\dot{Z}$  data.  
 124 The initial dataset, termed Dataset 1, was derived from annual means recorded  
 125 at 172 ground-based observatories for the year 1990. The SV is estimated over  
 126 12 months from July 1989 to June 1990. This assumes that there is little or  
 127 no secular acceleration relative to the size of the SV. Observation errors were  
 128 assigned to be a nominal  $1 \text{ nT/yr}$  for all stations and components. The second  
 129 dataset, termed Dataset 2, consisted of SV calculated by the same method as  
 130 Dataset 1, in this case from 176 ground-based observatories, but with a further  
 131 correction applied to remove internal covariance within the data (Wardinski  
 132 and Holme, 2006). The associated observation error for each component was  
 133 estimated by fitting a magnetic field model through a time series of data  
 134 from 1980–2000 and estimating the covariance of misfit to the model for each  
 135 direction. The errors ranged from 0.91 to  $103 \text{ nT/yr}$  for the  $X$  direction, with

136 a median value of  $3.8 \text{ nT/yr}$ . The  $Z$  direction was similarly distributed, while  
137 the  $Y$  direction had the smallest range of values. (The  $X$  and  $Z$  components  
138 are often inversely correlated, due to external field contamination.)

139 As ground-based observatories are unevenly geographically distributed, a third  
140 ‘global’ synthetic SV data set, consisting of 288 points on the globe sepa-  
141 rated by  $15^\circ$  intervals in latitude and longitude, was created. Dataset 3 was  
142 generated from the IGRF10 spherical harmonic model for the epoch 1990.0.  
143 The associated observation errors for Dataset 3 were also fixed at a nominal  
144  $1 \text{ nT/yr}$ .

145 The GUFM1 field model (Jackson et al., 2000) provided the main field coef-  
146 ficients for the Gaunt and Elsasser (i.e.  $\mathbf{B}$ ) matrices. Calculating toroidal- or  
147 poloidal-only flow models requires omission of either the Elsasser or Gaunt  
148 matrix in the formulation of  $\mathbf{B}$  and solving for the desired toroidal or poloidal  
149 coefficients respectively. The residual errors for the first iteration of the one-  
150 norm solution are obtained from an initial starting model calculated from a  
151  $L_2$  solution of the input data. The value of very small ( $< 10^{-4}$ ) error residuals  
152 in the matrix  $\mathbf{R}$  are set to  $10^{-4}$  to prevent the formation of ill-conditioned  
153 matrices, as advocated by Walker and Jackson (2000). No other nonunique-  
154 ness constraints were imposed on the solution. In common with Walker and  
155 Jackson (2000), 15-20 iterations were typically sufficient to ensure solution  
156 convergence. We find that the use of this  $L_1$  iterative method vastly improves  
157 the fit of the model to the data (using the measures in Equation 6 and the  
158 distribution of the residuals) compared to  $L_2$  minimisation, justifying the use  
159 of this approach.

160 **4 Comparison of Combined, Toroidal-only and Poloidal-only Flow**  
 161 **Models**

162 It has been recognised that toroidal-only flow models can often fit the data  
 163 adequately, though overall they do not fit well enough (Whaler, 1986). A small  
 164 poloidal component in the flow increases the number of degrees of freedom,  
 165 but makes a statistically significant improvement to the data fit. Typically,  
 166 the ratio of the energy of the toroidal to poloidal flow within a combined (i.e.  
 167 toroidal and poloidal) flow regime averages at approximately 0.85, under the  
 168 model assumptions from Section 2. An analysis of the individual contribution  
 169 of each flow coefficient shows that, though most of the flow energy is in the  
 170 toroidal coefficients, part of it is in the low degree and order coefficients of  
 171 the poloidal flow, even though overall the total poloidal flow contribution is  
 172 relatively small.

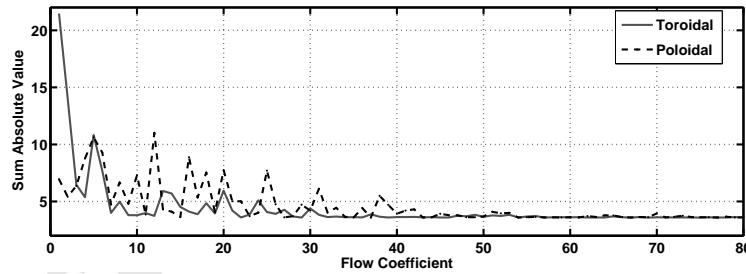


Fig. 1. The sum of the absolute values (SAV) of the residual when each coefficient indicated is not included in the toroidal-poloidal flow solution from Dataset 3. When all 448 coefficients are present, the SAV is 3.59. Coefficients are ordered  $t_1^0$ ,  $t_1^{1c}$ ,  $t_1^{1s}$ ,  $t_2^0$ ,  $t_2^{1c}$ , etc.

173 Figure 1 shows the sum of the absolute values (SAV) of the residual errors  
 174 from a one-norm solution in which an individual flow coefficient has been  
 175 removed and the resulting difference between the forward model and the ob-

176 served data is calculated. Coefficients are ordered  $t_1^0, t_1^{1c}, t_1^{1s}, t_2^0, t_2^{1c}$ , etc, with  
 177 the superscripts  $c$  and  $s$  denoting coefficients multiplying  $\cos m\phi$  and  $\sin m\phi$   
 178 respectively. With all 448 flow coefficients present, the SAV is 3.59. A higher  
 179 value thus indicates a worse fit to the data. It can be seen from Figure 1 that  
 180 excluding individual coefficients lower than degree and order 7 has the largest  
 181 effect on the solution, demonstrating that the flow has converged above de-  
 182 gree and order 8, and that some of the low degree and order poloidal terms  
 183 contribute significantly to the data fit. For example, solutions without  $s_3^{1c}$   
 184 (poloidal coefficient 12) fit worse than solutions without  $t_2^0$  (toroidal coeffi-  
 185 cient 4). This observation motivated the comparison of three different flow  
 186 types (i.e. combined, toroidal- and poloidal-only).

#### 187 4.1 Minimisation using the ‘Strong’ Velocity Norm

188 The results from experiments where the regularising constraint is the minimi-  
 189 sation of the ‘strong’ velocity norm (Equation (4)) are summarised in Table  
 190 1. The solution norm (the square root of Equation (4)) of all the models has  
 191 been set to  $2.6 \times 10^5 (km/yr)^2$ , by appropriate adjustment of the damping  
 192 parameter ( $\lambda$ ). This corresponds to equalising the ‘roughness’ of the com-  
 193 bined, toroidal- and poloidal-only flows for each dataset, making the three  
 194 flow regimes directly comparable. This value of the solution norm was chosen  
 195 to produce a flow model with a ‘reasonable’ RMS velocity of approximately  
 196  $16 km/yr$  for the combined toroidal-poloidal models.

197 The results from Dataset 1 indicate that the combined flow model has a far  
 198 better fit to the observatory data than the toroidal-only or poloidal-only mod-  
 199 els. Surprisingly, the poloidal-only flow model fits the data better than the

200 toroidal-only model (that is, the one-norm measure of error is smaller). For  
201 Datasets 2 and 3, the toroidal-only flow model fits the observations better  
202 than the poloidal-only model, but not by a large amount.

203 The average data misfit (defined as  $\sum |e_i|/N$ ) for both Datasets 1 and 3 is  
204 approximately  $10 \text{ nT/yr}$ . The combined flow model produced from Dataset 2  
205 has the lowest spread of residuals, thus giving the best overall fit. The average  
206 data misfit for Dataset 2 is  $1.1 \text{ nT/yr}$ . It is interesting to note that, despite  
207 the slower RMS flow velocities, poloidal-only models produce an adequate fit  
208 to the input SV data.

209 Figure 2 illustrates the three different flow models calculated from Dataset 2.  
210 The accompanying histograms show the residual errors i.e. the difference be-  
211 tween the flow model prediction of the SV at each observatory and the actual  
212 data recorded. From inspection of Table 1, it appears that the toroidal-only  
213 flow and the poloidal-only flow maintain an equally good fit to the observatory  
214 data, based on the one-norm and two-norm measures. However, comparison  
215 of the histograms of Figure 2 (*e*) and (*f*) indicates that the poloidal-only  
216 flow model is actually more strongly peaked about zero than the toroidal flow  
217 model. On the other hand, the poloidal-only model has a larger spread of resid-  
218 ual values leading to heavier tails than the toroidal-only flow model residuals.  
219 The flow patterns of the toroidal-only flow model are broadly similar to the  
220 combined model whilst the poloidal-only model has few visible similarities to  
221 the full combined model or the poloidal part of the combined flow.

222 Analysis of the geographical distribution of the residual errors for the flows  
223 reveals that the largest deviations occur in the  $\dot{X}$  component of the observatory  
224 data, concentrated in the northern regions of Asia and Europe.

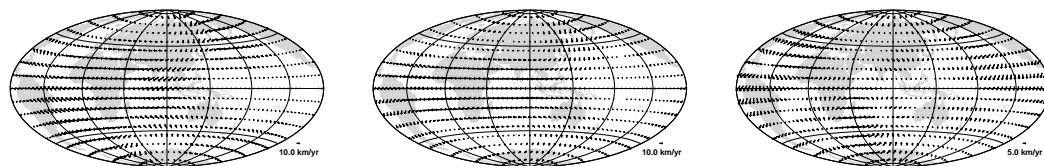
Dataset	Model	One-Norm	Two-Norm	Misfit	RMS Vel.
1	TorPol	4099	615	7.9	15.8
	Tor	6189	658	12	14.1
	Pol	6012	684	11.6	7.7
2	TorPol	366	30	0.7	16.6
	Tor	674	49	1.3	14.3
	Pol	695	58	1.3	7.9
3	TorPol	3108	199	3.6	15.5
	Tor	7792	406	9	13.3
	Pol	8600	499	9.9	7.5

Table 1

Fit of flow models to observatory SV data minimising the ‘strong’ velocity norm. The solution norm of each model is  $2.6 \times 10^5 (km/yr)^2$ . One-Norm, Two-Norm and Misfit are in  $nT/yr$ . RMS Velocity is in units of  $km/yr$ .

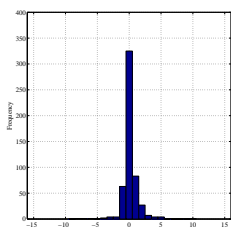
#### 225 4.2 Minimisation using the Root Mean Square SV Norm

226 The second set of experiments applied the regularising constraint of minimis-  
 227 ing the CMB RMS SV predicted by the model solutions. Due to numerical  
 228 instability, minimisation using this norm (Equation (5)) cannot be undertaken  
 229 directly. Following Whaler (1986) we added a flow constraint, with a very small  
 230 damping parameter,  $\mu$ , typically two orders of magnitude smaller than the SV  
 231 constraint damping parameter. The flow models from the three datasets were

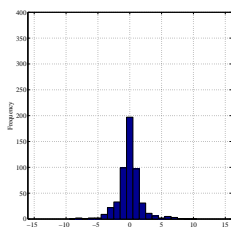


(a) Toroidal-Poloidal (b) Toroidal Flow Model (c) Poloidal Flow Model

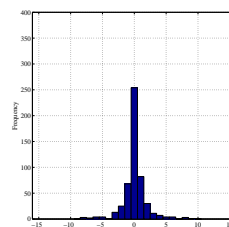
Flow Model



(d) Histogram of Flow Model Data Residuals



(e) Histogram of Flow Model Data Residuals



(f) Histogram of Flow Model Data Residuals

Fig. 2. Core-mantle boundary flow Models and Histograms of the residuals to the observatory SV data for Dataset 2 with the ‘strong’ velocity norm applied. Continents shown for reference.

232 solved in the same manner as previously, altering the values of  $\mu$  and  $\lambda$  until  
 233 the ‘strong’ velocity norms are equal. Table 2 summarises the results. The  
 234 velocity norm has to be set to a much higher value of  $5.8 \times 10^6 (km/yr)^2$  to  
 235 achieve a RMS velocity of approximately  $16 km/yr$  (for the combined flow).  
 236 With this value, the one-norm and two-norm misfit and RMS velocity metrics  
 237 of the solutions from the combined flows are comparable to those in Table  
 238 1. The toroidal-only and poloidal-only flows are, however, significantly poorer  
 239 than the solutions calculated with only the ‘strong’ velocity norm constraint.  
 240 Furthermore, the flow patterns and residual distributions (Figure 3) reveal  
 241 that the solutions are markedly different from those in Figure 2.

242 The effects of increased damping via  $\mu$  and  $\lambda$  to set the strong velocity norm

243 equal to  $2.6 \times 10^5 \text{ (km/yr)}^2$  (i.e. comparable to the value in Table 1) are shown  
 244 in Table 3. Extremely poorly fitting solutions are produced, compared to both  
 245 Tables 1 and 2. The flows minimising the ‘strong’ velocity norm converge  
 246 around degree 8. In contrast, the toroidal- and poloidal-only flow models  
 247 generated from the RMS SV constraint have no significant power in any par-  
 248 ticularly dominant degree (their spectra are almost flat), whilst the combined  
 249 models have some power in the lower degrees, but do not converge until degree  
 250 12.

251 The last column in Tables 2 and 3 gives the RMS SV generated on the CMB  
 252 for each model. Magnetic field models such as IGRF10 (Macmillan and Maus,  
 253 2005) and CHAOS (Olsen et al., 2006) predict values in the range  $60 - 70 \times$   
 254  $10^6 \text{ (nT/yr)}^2$ . The models in Table 1 behave in a similar manner, generating  
 255 SV values between 63 and  $200 \times 10^6 \text{ (nT/yr)}^2$ . As can be seen in Table 2,  
 256 combined flows generate only slightly higher SV than this for a similar RMS  
 257 velocity. In contrast, the SV generated by toroidal- and poloidal-only flows is  
 258 minuscule. For the models in Table 3, the SV generated is orders of magnitude  
 259 smaller. This is due to the extremely slow flow velocities, reflecting the fact  
 260 that the models are not vigorous enough to fit the data well, even though they  
 261 are complex (as reflected by their strong velocity norm value).

262 Allowing the toroidal- or poloidal-only models in Tables 2 and 3 to become  
 263 more realistic (by reducing the damping parameters) does generate SV values  
 264 similar to the standard magnetic field models, but at the cost of greatly in-  
 265 creased complexity of the flow. Thus, when using the RMS SV norm, simple  
 266 flows fit the data poorly, while very complex flows are needed to generate a  
 267 realistic amount of CMB SV and improve the fit to observations.

Dataset	Model	One-Norm	Two-Norm	Misfit	RMS Vel.	RMS SV
1	Tor+Pol	3925	195	7.6	15.3	239
	Tor	11966	882	23	5.1	0.08
	Pol	11519	865	22.3	5.3	0.1
2	Tor+Pol	343	29	0.6	16.0	268
	Tor	1628	112	3.1	5.1	0.07
	Pol	1618	111	3.1	5.3	0.1
3	Tor+Pol	2861	200	3.3	15.6	118
	Tor	18132	886	20.9	5.6	0.3
	Pol	17923	883	20.7	5.8	0.05

Table 2

Fit of flow models to observatory SV data minimising the Root-Mean-Square Secular Variation over the CMB. The ‘strong’ velocity norm value of each model is  $5.8 \times 10^6 (km/yr)^2$ . RMS CMB SV is in units of  $10^6 (nT/yr)^2$ . Other units as for Table 1.

## 268 5 Discussion

269 In this study we find a number of new results. Firstly, the allocation of the  
 270 error budget through the covariance matrix has a dramatic effect on the fit of  
 271 the flow to the observations. The observation errors for Datasets 1 and 3 have  
 272 been set equal; a simple but physically unrealistic allocation. In contrast, the  
 273 observation errors in Dataset 2, have been corrected for covariance between  
 274 the  $X$ ,  $Y$  and  $Z$  observatory components, to improve the removal of exter-

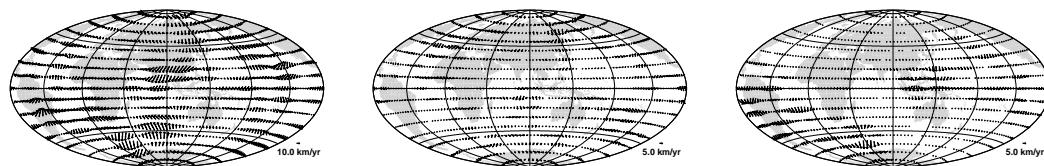
Dataset	Model	One-Norm	Two-Norm	Misfit	RMS Vel.	RMS SV
1	Tor+Pol	7632	722	14.8	3.9	1.4
	Tor	13811	955	26.8	1.1	0.0005
	Pol	13859	957	26.9	1.1	0.0003
2	Tor+Pol	971	75	1.8	3.9	1.4
	Tor	1808	121	3.4	1.2	0.02
	Pol	1824	122	3.5	1.2	0.02
3	Tor+Pol	15363	761	17.8	3.3	0.5
	Tor	23690	1123	27.4	1.0	0.003
	Pol	23478	1114	27.2	1.1	0.004

Table 3

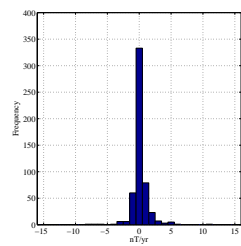
Fit of flow models to observatory SV data minimising the Root-Mean-Square Secular Variation over the CMB. The ‘strong’ velocity norm value has been matched to that of Table 1. Units as in earlier tables.

275 nal field contamination. Including additional information about data quality  
 276 through the covariance matrix leads to an improved fit. Tables 1 and 2, and  
 277 the histograms of residuals, indicate that Dataset 2 consistently achieves the  
 278 flow with the best fit to the SV input data.

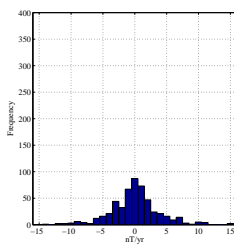
279 Secondly, the choice of solution norm alters the resultant flow pattern sig-  
 280 nificantly, despite an equivalently good fit. Minimisation using the ‘strong’  
 281 velocity norm (Figure 2) produces flows showing patterns similar to those  
 282 of other studies (e.g. Bloxham and Jackson, 1991; Waddington et al., 1995;



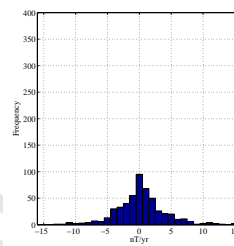
(a) Toroidal-Poloidal Flow Model (b) Toroidal Flow Model (c) Poloidal Flow Model



(d) Histogram of Flow Model Data Residuals



(e) Histogram of Flow Model Data Residuals



(f) Histogram of Flow Model Data Residuals

Fig. 3. Flow Models and Histograms of the residuals to the observatory  $SV$  data for Dataset 2 minimising the RMS  $SV$  predicted by the flow. Note the contrast with Figure 2.

283 Holme and Olsen, 2006). However, the flows resulting from minimising CMB  
 284 root-mean-square  $SV$  are more complex (Figure 3) and admit only combined  
 285 flow model solutions. They do not match the typical patterns found in other  
 286 core flow studies.

287 Thirdly, the existence of seemingly viable and relatively well-fitting poloidal-  
 288 only flow models is a surprising result (Figure 2), given that such flows are  
 289 currently considered physically unfeasible in the core dynamic regime. Note  
 290 that Dataset 3 consists of evenly geographically distributed ‘stations’, indi-  
 291 cating that the conclusions drawn here are not a function of the particular  
 292 distribution of observatories available.

293 Love (1999) developed a dynamo model in which poloidal-only flow dominates  
294 at the CMB. That particular dynamo model exhibited no SV at the surface,  
295 but does illustrate that such flows are theoretically possible. In contrast, our  
296 poloidal-only flows generate sufficient SV to explain the observations. However,  
297 Gubbins (2007) shows that strong poloidal flows would expel large amounts  
298 of toroidal flux from the core, thus undermining the frozen-flux hypothesis on  
299 which flow inversion is predicated. Our poloidal flows may be sufficiently weak  
300 to overcome this problem.

301 Combining these previous results with the findings from this study suggests  
302 that poloidal-only flows do not provide a good representation of the CMB flow,  
303 despite the relatively good fit to the SV data. Additionally, this work shows  
304 that CMB SV values matching those in standard models can be easily achieved  
305 with velocity norm regularised solutions. In contrast, SV norm regularised  
306 solutions produce complex flows for a comparable fit to the data with only  
307 slightly smoother CMB SV. Thus solutions minimising the SV norm have no  
308 real advantage over those with smooth flows.

## 309 **6 Conclusions**

310 We have employed an  $L_1$  error norm iterative minimisation method to invert  
311 SV data directly for core flow models. We find this approach improves the  
312 fit of the SV generated by the models to the observed data compared to the  
313 usual  $L_2$  (least-squares) norm. Using SV data rather than spherical harmonic  
314 SV models allows us to examine better the effects of some flow assumptions  
315 and constraints imposed upon inversions. Using two datasets of SV derived  
316 from ground-based observatories and a third consisting of synthetic SV on a

317 regular grid, it is shown that observation errors affect the overall fit of the  
318 flow model to the input data. In particular, using a dataset for which variable  
319 observation errors have been calculated for each component by co-estimation  
320 improves the overall fit (compared to models obtained assuming equal data  
321 errors).

322 The constraints normally imposed in a regularised inversion are also shown  
323 to influence greatly the resultant flow regime. A constraint which minimises a  
324 velocity norm of the flow is weaker (i.e. permits a ‘larger’ model space) than a  
325 constraint that minimises the CMB RMS SV predicted by the flow. The weaker  
326 constraint allows solutions such as poloidal-only flow models to exist which are  
327 equally as valid as toroidal-only flow models, in some cases producing a better  
328 fit to the input data. The stronger constraint produces complex flow regimes,  
329 which do not match the simpler flow patterns from the weaker constraint  
330 or results from other studies. Therefore, it probably has little use beyond  
331 hypotheses testing frozen-flux and flow modelling assumptions. We therefore  
332 recommend CMB flows are derived by the  $L_1$  norm minimisation method with  
333 a velocity norm constraint.

### 334 **Acknowledgements**

335 We would like to thank Ingo Wardinski for sharing the covariance corrected  
336 secular variation dataset. We also thank Richard Holme and Andrew Jackson  
337 for useful discussion of this work and Susan Macmillan for constructive com-  
338 ments on the manuscript. Part of this work was presented at a meeting organ-  
339 ised by Keke Zhang to celebrate the 60th birthday of David Gubbins, one of the  
340 pioneers of modern geomagnetism. We thank David Gubbins for helpful com-

341 ments on an earlier version of this manuscript. KAW acknowledges his advice,  
342 encouragement and support throughout her career. This research is part of the  
343 NERC GEOSPACE programme, funded under grant NER/O/S/2003/00674.  
344 CDB is funded under NERC studentship award NER/S/J/2005/13496.

## 345 **References**

- 346 Amit, H., Olson, P., 2004. Helical core flow from geomagnetic secular variation.  
347 *Phys. Earth Planet. Int.* 147, 1–25.
- 348 Backus, G. E., 1968. Kinematics of geomagnetic secular variation in a perfectly  
349 conducting core. *Philos. Trans. R. Soc. Lond. Ser A* 263, 239–266.
- 350 Bloxham, J., 1988. The determination of fluid flow at the core surface from  
351 geomagnetic observations. Vol. *Mathematical Geophysics*. D. Reidel Pub-  
352 lishing Company, Ch. 9, pp. 189–208.
- 353 Bloxham, J., Jackson, A., February 1991. Fluid flow near the surface of Earth’s  
354 outer core. *Reviews of Geophysics* 29, 1, 97–120.
- 355 Braginsky, S., LeMouël, 1993. Two-scale model of a geomagnetic field varia-  
356 tion. *Geophys. J. Int.* 112, 147–158.
- 357 Gubbins, D., 1983. Geomagnetic field analysis - I. Stochastic inversion. *Geo-*  
358 *phys. J. R. Astr. Soc.* 73 (3), 641–652.
- 359 Gubbins, D., 2007. Geomagnetic constraints on stratification at the top of the  
360 Earth’s core. *Earth Planets Space* 59, 661–664.
- 361 Gubbins, D., Kelly, P., 1996. A difficulty with using the frozen flux hypothesis  
362 to find steady core motions. *Geophys. Res. Lett.* 23 (14), 1825–1828.
- 363 Hills, R., 1979. Convection in the earth’s mantle due to viscous shear at the  
364 core-mantle interface and due to large-scale bouyancy. Ph.D. thesis, N.M.  
365 State Univ., Las Cruces.

- 366 Holme, R., Olsen, N., 2006. Core surface flow modelling from high-resolution  
367 secular variation. *Geophys. J. Int.* 166, 518–528.
- 368 Jackson, A., Jonkers, A., Walker, M., 2000. Four centuries of geomagnetic secu-  
369 lar variation from historical records. *Philos. Trans. R. Soc. Lond.* 358 (1768),  
370 957–990.
- 371 Kahle, A., Vestine, E., Ball, R., 1967. Estimated surface motions of the Earth's  
372 core. *J. Geophys. Res.* 72, 1095–1108.
- 373 Le Mouél, J., 1984. Outer-core geostrophic flow and secular variation of Earth's  
374 geomagnetic field. *Nature* 311, 734 – 735.
- 375 Love, J., 1999. A critique of frozen-flux inverse modelling of a nearly steady  
376 geodynamo. *Geophys. J. Int.* 138, 353–365.
- 377 Macmillan, S., Maus, S., 2005. International geomagnetic reference field:the  
378 tenth generation. *Earth Planets Space* 57, 1135–1140.
- 379 Olsen, N., Luhr, H., Sabaka, T., Manda, M., Rother, M., Toffner-Clausen,  
380 L. a., 2006. Chaos: a model of the earth's magnetic field derived from champ,  
381 rsted, and sac-c magnetic satellite data. *Geophys. J. Int.* 166, 67–75.
- 382 Roberts, P., Scott, S., 1965. On the analysis of the secular variation. 1. A  
383 hydromagnetic constraint: Theory. *J. Geomag. Geoelec.* 17, 137–151.
- 384 Voorhies, C., Backus, G., 1985. Steady flows at the top of the core from ge-  
385 omagnetic field models: The steady motion theorem. *Geophys. Astrophys.*  
386 *Fluid Dynam.* 32, 163–173.
- 387 Waddington, R., Gubbins, D., Barber, N., 1995. Geomagnetic field analysis -  
388 V. Determining steady core-surface flows directly from geomagnetic obser-  
389 vations. *Geophys. J. Int.* 122 (1), 326–350.
- 390 Walker, M., Jackson, A., 2000. Robust modelling of the Earth's magnetic field.  
391 *Geophys. J. Int.* 143-3, 799–808.
- 392 Wardinski, I., Holme, R., 2006. A time-dependent model of the earth's mag-

- 393 netic field and its secular variation for the period 1980-2000. *J. Geophys.*  
394 *Res.* 111, B12101.
- 395 Whaler, K., 1980. Does the whole of the Earth's core convect? *Nature* 287,  
396 528–530.
- 397 Whaler, K. A., 1986. Geomagnetic evidence for fluid upwelling at the core-  
398 mantle boundary. *Geophys. J. R. Astr. Soc.* 86, 563–588.
- 399 Whaler, K. A., 2007. *Encyclopedia of Geomagnetism and Paleomagnetism.*  
400 Springer, Dordrecht, Ch. Core Motions, pp. 84–89.